

Distant Field BHB Stars III: Identification of a probable outer halo stream at Galactocentric distance $r = 70$ kpc

L. Clewley¹*, S. J. Warren², P. C. Hewett³, John. E. Norris⁴, M. I. Wilkinson³, N. W. Evans³

¹Department of Physics, Denys Wilkinson Bldg., University of Oxford, Keble Road, Oxford, OX1 3RH

²Blackett Laboratory, Imperial College of Science Technology and Medicine, Prince Consort Road, London SW7 2BW

³Institute of Astronomy, Madingley Road, Cambridge CB3 0HA

⁴Research School of Astronomy & Astrophysics, The Australian National University, Mount Stromlo Observatory, Cotter Road, Weston, ACT 2611, Australia

Released 2002 XXXXX XX

ABSTRACT

We present VLT-FORS1 spectra of a sample of 34 faint $20.0 < g^* < 21.1$ A-type stars selected from the Sloan Digital Sky Survey Early Data Release, with the goal of measuring the velocity dispersion of blue horizontal branch (BHB) stars in the remote Galactic halo, $R \sim 80$ kpc. We show that colour selection with $1.08 < u^* - g^* < 1.40$ and $-0.2 < g^* - r^* < -0.04$ minimises contamination of the sample by less luminous blue stragglers. In classifying the stars we confine our attention to the 20 stars with spectra of signal-to-noise ratio $> 15\text{\AA}^{-1}$. Classification produces a sample of eight BHB stars at distances $65 - 102$ kpc from the Sun (mean 80 kpc), which represents the most distant sample of Galactic stars with measured radial velocities. The dispersion of the measured radial component of the velocity with respect to the centre of the Galaxy is $58 \pm 15\text{km s}^{-1}$. This value is anomalously low in comparison with measured values for stars at smaller distances, as well as for satellites at similar distances. Seeking an explanation for the low measured velocity dispersion, further analysis reveals that six of the eight remote BHB stars are plausibly associated with a single orbit. Three previously known outer halo carbon stars also appear to belong to this stream. The velocity dispersion of all nine stars relative to the orbit is only $15 \pm 4\text{km s}^{-1}$. Further observations along the orbit are required to trace the full extent of this structure on the sky.

Key words: Galaxy: halo – stars: horizontal branch – Galaxy: structure – Galaxy: stream

1 INTRODUCTION

The existence of a dark massive halo appears to be a generic feature of many galaxies, but the total masses, sizes, and the formation history of galactic halos are poorly understood. This is mostly because we do not have large enough samples of dynamical tracers at sufficiently large radii. The formation and extent of such mass distributions are of great importance in understanding the nature of the dark matter and its role in galaxy formation and evolution. For instance, the quantification of the dark matter content of the Galaxy would allow us to construct a picture of the assembly of the various baryonic components, through comparison with simulations. The baryonic components can, in turn, provide information about the evolution of the halo.

There is compelling evidence that at least part of the stellar halo has been built up via the accretion of smaller satellite galaxies. Numerous searches have been made for streams of material responsible for building up the Galaxy. A striking example is the identification of the Sagittarius dwarf galaxy (Ibata, Gilmore & Irwin, 1994) and its stellar stream (e.g. Helmi & White, 2001). Recently, an extensive stream of stars has been uncovered in the halo of the Andromeda galaxy (M31), revealing that it too is cannibalising a small companion (e.g. Lewis et al. 2004). Such streams yield crucial information on the accretion history and formation of galaxy halos. Extended stellar streams have also been used to constrain the mass of the Galactic halo (e.g. Johnston et al. 1999) and in M31 (Ibata et al. 2004). A number of authors have noted the possible evidence for streams in the distribution of the intrinsically rare, but very luminous, carbon stars. Sanduleak (1980) proposed the association of

* E-mail: clewley@astro.ox.ac.uk

a single carbon star with the Magellanic Stream and Totten & Irwin (2000) made the general observation that the non-uniform distribution of carbon-stars in their extensive survey of the halo may indicate that a number of the stars are associated with streams.

We have previously argued (Clewley et al., 2002, hereafter Paper I) that blue horizontal branch (BHB) stars are an ideal population for exploring the outer reaches of the Halo. Like carbon stars they are luminous standard candles but are also far more numerous.

BHB stars are A-type giants. A-type stars in the Galactic halo are easily identified, as they lie blueward of the main-sequence turnoff (e.g. Yanny et al., 2000, hereafter Y2000). Unfortunately assembling clean samples of remote $r > 60$ kpc¹ BHB stars is made difficult by the existence of a contaminating population of high-surface-gravity A-type stars, the blue stragglers, that are between one and three mag. fainter. Previous analyses required high signal-to-noise ratio (S/N) spectroscopy to reliably separate these populations (e.g. Kinman, Suntzeff, and Kraft, 1994), making identification of BHB stars in the distant halo unfeasible.

This paper is the third in a series. In Paper I we developed two classification methods that enabled us to overcome the difficulties in cleanly separating BHB stars from blue stragglers, and outlined an observational programme to survey the halo for BHB stars. In the second paper (Clewley et al., 2004, hereafter Paper II), we presented photometry and spectroscopy of faint $16.0 < B < 19.5$ candidate BHB stars in two northern high Galactic latitude fields and four southern fields. This work resulted in a sample of 60 BHB stars at distances $11 < R < 52$ kpc (mean 28 kpc), with measured radial velocities. Here we apply the methods of Papers I and II to survey for halo BHB stars at much greater distances, $65 < R < 115$ kpc. The new survey uses Sloan Digital Sky Survey (SDSS) photometry to isolate a sample of faint halo A-type stars. Reliable classifications are derived from medium resolution spectroscopy using FORS1 at the VLT.

The candidate BHB stars observed at the VLT were selected using $u^*g^*r^*$ photometry from the SDSS Early Data Release (EDR) data set (Stoughton et al., 2002). The EDR photometry was preliminary, and has since been revised. Because we need accurate Johnson-Kron-Cousins B, V magnitudes for the classification, we have used the more recent SDSS Data Release 2 (DR2) photometry (Abazajian, 2004) of the EDR-selected candidates for this purpose. In Section 2 of this paper we describe the selection of the BHB candidates from the EDR data set, and provide our prescription for transforming the DR2 g, r magnitudes of A-type stars to B, V magnitudes. Section 3 provides a summary of the VLT spectroscopic observations, and the data reduction and line measurement procedures followed. In Section 4 we use the methods of Papers I and II to classify these stars into categories BHB and blue straggler, and provide a summary table of distances and radial velocities of the eight stars classified as BHB. We compute the velocity dispersions of the two populations and compare them with previous work. In Section 5 we discuss the kinematics of the BHB stars. We

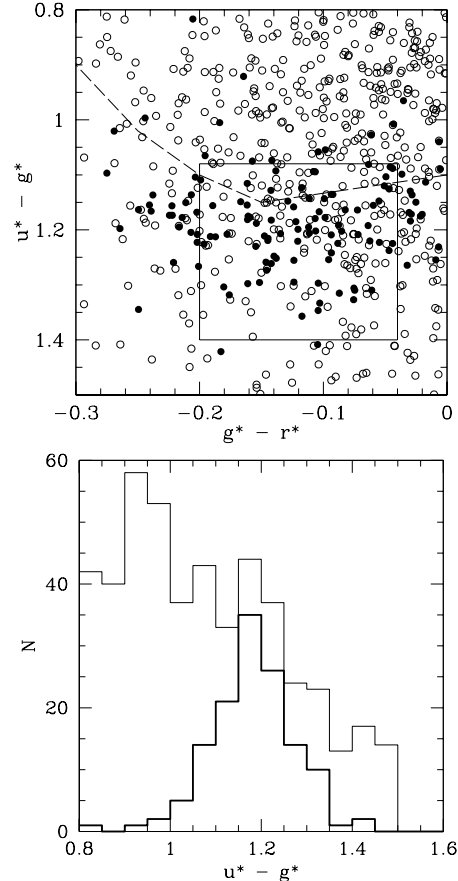


Figure 1. *Upper:* Two colour plot of stellar objects in SDSS stripe 10, in the RA range $200^\circ < \alpha < 230^\circ$, the region including the Sagittarius tidal stream. Filled circles mark objects in the apparent magnitude range $18.8 < g^* < 19.2$, expected to be predominantly BHB stars. Open circles mark objects in the apparent magnitude range $20.5 < g^* < 21.5$, expected to be predominantly blue stragglers. The box marks our adopted colour selection. The dashed line marks the division between high and low gravity A stars employed by Y2000. *Lower:* Histograms of the $u^* - g^*$ colours of the stars in the upper plot. The thick line corresponds to the filled circles, and the thin line to the open circles. Typical colour errors for these two samples are $\sigma(u^* - g^*) = 0.05$ and 0.20, respectively.

perform an orbital analysis of the sample and suggest that most of them are plausibly associated with a single orbit.

2 SELECTING THE BHB CANDIDATES

2.1 Colour selection

We selected candidate BHB stars using the SDSS EDR point spread function (PSF) $u^*g^*r^*$ magnitudes of stellar objects. The SDSS photometry has evolved between EDR and DR2 for a variety of reasons: i) the reference photometric system is now that of the SDSS 2.5m telescope itself, rather than the photometric monitoring telescope, ii) the absolute calibration of the standards has improved, and the calibration of the survey data relative to the standards has improved, iii) instrumental systematics (especially scattered light) are

¹ In this paper we use the coordinate r to denote Galactocentric distances and the coordinate R to denote heliocentric distances.

now better understood. Therefore, we have taken advantage of the improved photometry in DR2 for the subsequent analysis, in particular in classifying the objects and estimating their distances. To distinguish between photometric systems, the EDR system is designated by asterisks, the system of the photometric monitoring telescope is designated by primes, and the DR2 magnitudes are unadorned, which is the SDSS convention. Bearing in mind that all the stars are in the remote halo, all the SDSS magnitudes discussed in this paper have been corrected for Galactic extinction, using the map of Schlegel, Finkbeiner & Davis (1998).

We limited ourselves to the northern equatorial stripe in the EDR data set, which covers $145^\circ < \alpha < 236^\circ$, $-1.25^\circ < \delta < +1.25^\circ$ (J2000). This is SDSS stripe 10, observed in runs 752 and 756 (Stoughton et al., 2002). In selecting candidate distant BHB stars from the EDR, we were guided by the results of Y2000, who studied the spatial distribution of a sample of A-type stars selected from the EDR using the (reddening-corrected) colour selection box $-0.3 < g^* - r^* < 0.0$, $0.8 < u^* - g^* < 1.5$. In plotting apparent magnitude against α for these A-type stars, Y2000 discovered that the distribution is not smooth, but includes striking over-dense regions occurring in bands. These have subsequently been identified as tidal debris from the Sagittarius dwarf galaxy. Furthermore the bands occur in pairs, coincident on the sky, but separated by ~ 2 mag. The brighter objects are the more luminous BHB stars, and the fainter objects are blue stragglers at the same spatial location in the halo.

Our aim was to use the EDR data set to select a sample of candidate faint BHB stars, with minimal contamination by blue stragglers, in order to make the most efficient use of the spectroscopic time awarded (for classification and velocity measurement). To reach large distances, we chose the magnitude range $20.0 < g^* < 21.1$, corresponding to $\sim 65 < R < \sim 115$ kpc, if the objects are BHB stars. Fortunately, as demonstrated by Lenz et al. (1998) using synthetic photometry, the $u^*g^*r^*$ colours of A-type stars show some dependence on surface gravity. Given the accuracy of the photometry at the distances of interest, ~ 0.1 mag., the $u^*g^*r^*$ colours cannot provide *reliable* separation of the two populations. Nevertheless Y2000 demonstrated that a colour cut in the $u^* - g^*$ *versus* $g^* - r^*$ plane is effective in enhancing the contrast of the individual bands of tidal debris i.e. can substantially reduce the contamination of one population by the other.

Another way of looking at this is illustrated in Fig. 1. The upper diagram plots the colours of all EDR stars within the colour selection box of Y2000, for the limited range $200^\circ < \alpha < 230^\circ$, which is the region of the EDR containing the strongest tidal debris bands. Stars in the brighter band $18.8 < g^* < 19.2$, which should be predominantly BHB stars, are marked with solid symbols, while stars in the fainter band $20.5 < g^* < 21.5$, which should be predominantly blue stragglers, are marked with open symbols². For reference the dashed line shows the dividing line used by Y2000. The brighter band, typical colour error $\sigma(u^* - g^*) = 0.05$, is mostly confined to a narrow range

² The larger magnitude interval selected is because blue stragglers have a larger spread in luminosity than BHB stars (§3.2).

in $u^* - g^*$, which evidently defines the colour domain of the BHB stars. The fainter stars, open symbols, are concentrated towards the top of the plot, but are spread over a larger colour range. However, much of the spread is accounted for by the larger colour errors $\sigma(u^* - g^*) = 0.2$, as can be seen by reference to the histogram in the lower plot. It is evident that the mean $u^* - g^*$ colour of blue stragglers is substantially bluer than for BHB stars.

The spectroscopic classification criteria (detailed in §4) work best near $(B - V)_0 = 0.1$, which corresponds to $g^* - r^* = -0.125$, using the colour transformation provided by Fukugita et al. (1996). On this basis we adopted the colour cuts shown by the box in Fig. 1, defined by $1.08 < u^* - g^* < 1.40$, $-0.2 < g^* - r^* < -0.04$, and limited candidate selection to objects with colour error $\sigma(g^* - r^*) < 0.07$. While these colour cuts should be nearly optimal in terms of the fraction of candidates that are BHB stars, we would still expect substantial contamination by blue stragglers, on account of the large $u^* - g^*$ colour errors at the faint magnitudes of the sample, $20.0 < g^* < 21.1$.

The distribution in α and g^* of all the stars satisfying these criteria is shown in Fig. 2. The higher density of points at $\alpha > 200^\circ$ is due to blue stragglers in the Sagittarius tidal stream. Our classification methods produce samples of BHB stars that are contaminated by blue stragglers at the level of $< 10\%$, for samples of A-type stars with a typical mix of the two populations (Paper I). The contamination of our BHB sample would be substantially greater if we attempted to classify stars in this region, so we confined our sample to $\alpha < 200^\circ$. The clump visible at $\alpha = 153^\circ$, $g^* \sim 20.2$, is the horizontal branch of the Sextans dwarf spheroidal³, centre $\alpha = 153.3^\circ$, $\delta = -1.61^\circ$, J2000 (Irwin and Hatzidimitriou, 1995). In order to avoid stars in Sextans we confined our selection to $\alpha > 160^\circ$. The final selection includes 54 objects, of which we observed the 35 listed in Table 1. One of these, no. 32, proved to be a quasar. Looking ahead, of the remaining 34 candidates we are able to classify 20. These classifications are indicated on Fig. 2, with solid circles representing the eight stars classified BHB, and open circles representing the 12 stars classified blue straggler. For the remaining 14 candidates the classifications are uncertain, mostly due to insufficient S/N .

In Table 1 we provide details of the 35 objects observed. Column 1 is our running number, and column 2 lists the coordinates. Successive columns provide the dereddened DR2 g magnitude, and the dereddened $u - g$ and $g - r$ colours. The last column provides the dereddened $B - V$ colour, calculated using the transformation derived in §2.2. There is good agreement between the EDR and DR2 photometry in the mean, but with noticeable scatter. For example, looking at the difference $(g^* - r^*) - (g - r)$ for our targets, the mean is 0.00 mag., and the standard deviation is 0.03 mag.

2.2 Transforming from $g - r$ to $B - V$

We use two methods to classify stars into categories BHB star and blue straggler. One method makes use of $(B - V)_0$ colours. Therefore we need to convert the extinction

³ Note that the discussion in Y2000 of these objects mistakenly cites a paper concerned with a different galaxy, Sextans A.

No.	Identification (J2000)	<i>g</i>	$(u - g)_0$	$(g - r)_0$	$(B - V)_0$
01	J105319.31 + 004842.79	20.09 ± 0.02	1.08 ± 0.09	-0.08 ± 0.03	0.15 ± 0.03
02	J105322.38 – 004449.73	20.19 ± 0.03	0.81 ± 0.16	-0.10 ± 0.05	0.14 ± 0.04
03	J110639.10 – 004720.06	20.16 ± 0.03	1.11 ± 0.15	-0.13 ± 0.05	0.11 ± 0.04
04	J112352.91 – 003719.83	20.01 ± 0.02	1.33 ± 0.11	-0.16 ± 0.03	0.09 ± 0.03
05	J112744.35 + 001508.47	20.85 ± 0.03	1.29 ± 0.18	-0.14 ± 0.05	0.11 ± 0.04
06	J113050.42 – 005147.11	20.27 ± 0.04	1.03 ± 0.10	-0.14 ± 0.05	0.11 ± 0.04
07	J113407.58 – 004735.65	20.21 ± 0.04	1.28 ± 0.19	-0.06 ± 0.06	0.18 ± 0.04
08	J114818.87 – 003921.03	20.06 ± 0.05	1.10 ± 0.15	-0.08 ± 0.07	0.16 ± 0.05
09	J115525.99 – 003601.66	20.96 ± 0.03	1.27 ± 0.24	-0.08 ± 0.06	0.16 ± 0.04
10	J120024.18 + 011026.81	21.06 ± 0.04	1.28 ± 0.24	-0.13 ± 0.07	0.12 ± 0.05
11	J120855.70 + 010929.20	20.35 ± 0.03	1.18 ± 0.12	-0.14 ± 0.04	0.10 ± 0.04
12	J121447.45 + 004001.27	21.00 ± 0.04	1.15 ± 0.17	-0.10 ± 0.06	0.14 ± 0.05
13	J122305.31 – 011443.14	20.75 ± 0.04	1.22 ± 0.21	-0.10 ± 0.07	0.14 ± 0.06
14	J122726.77 + 004641.03	21.01 ± 0.03	1.16 ± 0.18	-0.09 ± 0.06	0.15 ± 0.05
15	J122802.26 – 010353.91	20.93 ± 0.05	1.10 ± 0.22	-0.11 ± 0.08	0.13 ± 0.06
16	J123805.94 + 001941.07	21.04 ± 0.04	1.13 ± 0.22	-0.06 ± 0.07	0.17 ± 0.05
17	J124112.31 – 010447.12	21.03 ± 0.04	1.06 ± 0.22	-0.06 ± 0.07	0.17 ± 0.06
18	J124620.96 – 002802.04	20.13 ± 0.02	1.26 ± 0.12	-0.20 ± 0.04	0.06 ± 0.03
19	J124851.75 + 003045.08	20.05 ± 0.02	1.21 ± 0.10	-0.07 ± 0.04	0.17 ± 0.03
20	J125004.94 + 003422.85	20.91 ± 0.04	1.14 ± 0.22	-0.10 ± 0.06	0.14 ± 0.05
21	J125054.28 – 000759.84	20.44 ± 0.03	1.12 ± 0.11	-0.17 ± 0.04	0.08 ± 0.04
22	J125123.59 + 000345.91	20.78 ± 0.03	1.01 ± 0.15	-0.11 ± 0.05	0.13 ± 0.04
23	J125308.36 – 000554.68	20.75 ± 0.03	1.20 ± 0.17	-0.08 ± 0.05	0.15 ± 0.04
24	J125336.47 – 002414.48	20.01 ± 0.03	1.16 ± 0.09	-0.14 ± 0.04	0.11 ± 0.03
25	J125934.17 + 002058.64	21.07 ± 0.04	1.00 ± 0.22	-0.07 ± 0.07	0.17 ± 0.06
26	J125938.97 + 000748.09	21.07 ± 0.04	1.56 ± 0.32	-0.10 ± 0.07	0.14 ± 0.05
27	J130528.14 + 004855.90	20.23 ± 0.04	1.14 ± 0.11	-0.06 ± 0.05	0.17 ± 0.04
28	J130907.25 + 005731.22	20.11 ± 0.03	1.16 ± 0.11	-0.10 ± 0.05	0.14 ± 0.04
29	J131109.31 + 000950.36	20.67 ± 0.03	1.28 ± 0.20	-0.18 ± 0.05	0.07 ± 0.04
30	J131155.98 + 003914.93	20.61 ± 0.03	0.84 ± 0.13	-0.11 ± 0.05	0.13 ± 0.04
31	J131252.50 + 000821.47	20.72 ± 0.03	1.05 ± 0.16	-0.13 ± 0.05	0.11 ± 0.04
32	J131435.78 + 010329.82Q	20.55 ± 0.03	0.98 ± 0.16	0.01 ± 0.06	0.22 ± 0.04
33	J131458.12 – 004706.39	20.30 ± 0.03	1.11 ± 0.14	-0.08 ± 0.04	0.15 ± 0.04
34	J131538.01 – 010853.30	20.26 ± 0.03	1.25 ± 0.13	-0.08 ± 0.04	0.16 ± 0.04
35	J131602.90 + 010150.60	20.50 ± 0.03	1.24 ± 0.17	-0.10 ± 0.05	0.14 ± 0.04

Table 1. Photometric data for the 35 BHB candidates from the SDSS DR2. One candidate that was subsequently found to be a quasar has ‘Q’ appended to the SDSS identifier.

corrected $g - r$ colours to $B - V$. Fukugita et al (1996) quote the transformation

$$B - V = (g' - r' + 0.23)/1.05, \quad (1)$$

computed from synthetic photometry. Smith et al. (2002) quote the transformation

$$B - V = (g' - r' + 0.19)/0.98, \quad (2)$$

based on observations of standard stars. These two relations are plotted in Fig. 3, as the dashed and dotted lines respectively. The two linear relations differ somewhat even over the narrow range of colours of interest in this paper, $-0.2 < g - r < -0.04$, by some 0.03 mag. Whereas one would naturally prefer the empirical relation over the synthetic relation, there is some indication that the actual transformation is non-linear in the region of the A stars, as the four stars measured by Smith et al. (2002) in the colour range of interest, lie on average 0.04 mag. above the linear relation (which is a fit over a wide colour range). Further evidence that the relation is non-linear comes from our own photometry, which is less precise, but has many more stars. Plotted in Fig. 1 are the colours of the 60 stars in the colour range $-0.05 < (B - V)_0 < 0.40$, with $(B - V)_0$ measured by our-

selves (Paper II), which also have SDSS DR2 $g - r$ colours. Only the errors on $(B - V)_0$ are plotted, as these dominate. Our data points are systematically high relative to the linear relation of Smith et al. (2002). An additional source of uncertainty is the fact that the above linear relations were derived for the $u'g'r'i'z'$ system of the photometric monitoring telescope, slightly different from the $ugriz$ system of the SDSS 2.5m telescope itself, used for DR2.

Accurate $(B - V)_0$ photometry is required for the classification of the stars using the $D_{0.15}$ -Colour method (§4). A systematic error in the $(B - V)_0$ colour as large as 0.05 mag. could result in many of the classifications being in error. Therefore we re-investigated the colour transformation. We computed synthetic colours using the methods detailed in Hewett et al. (in prep.). We used model stars with $[\text{Fe}/\text{H}] = -1$ and $\log g = 3.5$ (an appropriate surface gravity midway between BHB stars and blue stragglers), from Kurucz (1993). We fit a cubic polynomial to the relation between the $(B - V)_0$ and $(g - r)_0$ synthetic colours, for the colour range of Fig. 3. Finally, bearing in mind the uncertainty in the absolute calibration of the SDSS magnitudes onto the AB system (Fukugita et al., 1996), we allowed the zero point of the relation to be a free parameter, established

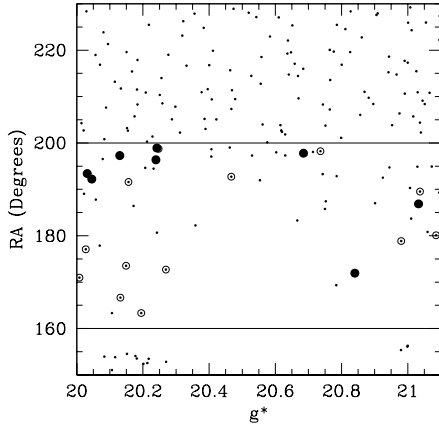


Figure 2. A plot of α against g^* for all the BHB star candidates in EDR stripe 10, satisfying our selection criteria (detailed in the text). Selection was confined to the range $160^\circ < \alpha < 200^\circ$. There are 54 stars satisfying the selection criteria, of which the 35 listed in Table 1 were observed and 20 were classifiable. The eight stars classified as BHB stars are marked by filled circles, and the 12 stars classified as blue stragglers are marked by open circles.

by shifting the derived curve vertically to give the best fit to the data of Fig. 3. The curve provides a better fit than the two linear relations plotted. Furthermore the average offset of the four stars measured by Smith et al. (2002) in the colour range of interest reduces to 0.005 mag. We have therefore adopted this relation. The transformation is given by

$$B-V = 0.764(g-r) - 0.170(g-r)^2 + 0.715(g-r)^3 + 0.218, \quad (3)$$

and is plotted in Fig. 3 as the bold solid line. We stress that this relation is specifically for A-type stars, and is not expected to be reliable for other types of star. The adjustment to the zero point was very small, only 0.014 mag. The agreement is encouragingly good and gives considerable confidence in the many elements going into this comparison – the SDSS DR2 photometry, the absolute calibration of Vega, and of the SDSS standard stars, our own photometry, the measurement of the different passband response functions, and the synthetic stellar spectra. The computed $(B-V)_0$ colours of our targets are listed in the final column of Table 1.

In summary, we have presented evidence that, in the colour range of interest, A stars lie systematically off the simple linear colour transformation measured by Smith et al. (2002), by about 0.05 mag. and we have derived a cubic relation that provides an improved fit.

3 SPECTROSCOPIC OBSERVATIONS, ANALYSIS, AND RESULTS

3.1 Observations

We used the VLT FORS1 instrument, in service mode, over two periods, from 2003/03/25 to 2003/04/09, and from 2004/01/30 to 2004/03/20, to obtain medium resolution optical spectra of the 35 BHB candidates. The instrument is equipped with a 2048^2 Tek CCD, with a projected scale of

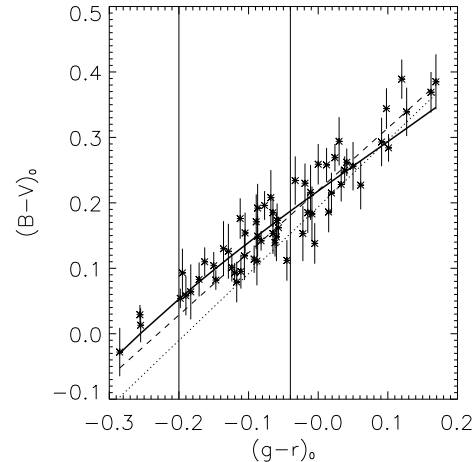


Figure 3. Colour transformation between dereddened SDSS DR2 $(g-r)_0$ colour and $(B-V)_0$. The data plot the photometry of the 60 stars from Paper II with SDSS photometry. The dashed line is the transformation derived by Fukugita et al. (1996) from synthetic photometry, and the dotted line is the transformation measured by Smith et al. (2002). The solid line is the cubic relation derived here from synthetic colours of Kurucz (1993) model stars. The vertical lines mark the $(g^*-r^*)_0$ colour selection limits.

$0.2''/\text{pixel}^{-1}$. We used the 600B grating, giving a dispersion of $1.2 \text{ \AA pixel}^{-1}$. With the $0.7''$ slit, the resolution achieved, measured from arc lines, was about 4 \AA , which is sufficient for the line-fitting procedure. The spectral coverage was 3400 – 5700 \AA , which includes the relevant lines $H\delta$, $H\gamma$, and $\text{Ca II K } \lambda 3933 \text{ \AA}$. Three BHB radial velocity standard stars in the globular cluster M5 were observed twice each. Table 2 summarises relevant information on the standards. Columns (1) to (5) list the identification, RA and Dec., V magnitude, $(B-V)_0$ colour, and the heliocentric radial velocity, V_\odot . The information in successive columns (6) to (11) in Table 3 contains averages of $H\delta$ and $H\gamma$ line measurements. Columns (6) to (8) in Table 2 list, respectively, the parameters $D_{0.15}$, b , and c (explained in §4). The errors on the parameters b and c are provided in columns (9) to (11) in the form of A and B , the semi-major and semi-minor axes of the error ellipse in the b – c plane, and θ the orientation of the semi-major axis, measured anti-clockwise from the b -axis. Here the error corresponds to the 68% confidence interval for each axis in isolation (see Paper I for further details).

The requested integration times of between 765 and 1980 seconds, for stars in the magnitude range $20.0 < g^* < 21.1$, were estimated using the FORS1 exposure-time calculator, on the basis of the requested seeing, transparency, and lunar phase, in order to achieve the minimum continuum S/N ratio of 15 \AA^{-1} required to classify the stars (Paper I). All targets were observed near culmination, with a mean airmass of 1.20 ± 0.1 . In the event, observations of 12 of the 34 targets failed to achieve the required S/N , and therefore these targets cannot be reliably classified. The failures were primarily in the cases where the seeing was poor. In retrospect, for these service observations we should have included a safety margin in the requested integration times. All im-

age frames were automatically bias and flat-field corrected by the FORS pipeline, and we then followed standard procedures for sky subtraction, spectral extraction, and wavelength calibration. An error spectrum, used for the line profile fits, was computed from Poisson considerations.

For the wavelength calibration, HgCdHe arc observations were made during the day, and were used to derive the dispersion solution. To account for any flexure of the instrument, the zero point of the dispersion solution was established for each spectrum using the [OI] night-sky line at 5577.34 Å. We found a *rms* drift of the zero point of 13 km s⁻¹ over the entire data set.

3.2 Analysis

As stated earlier, one of the candidates proved to be a quasar. In the remainder of the paper we ignore this object, and refer only to the 34 stars. The spectra were used to measure the shapes and widths of the H δ and H γ lines (for classification), the EW of the CaII K line (to measure the metallicity), and the radial velocity of each star (for future dynamical analysis). For these measurements we followed the procedures set out in Papers I and II exactly, and we refer the reader to those papers for full details. Below we provide a brief explanation of how the Balmer lines were measured, and how the CaII K line EW is used to determine the metallicity. We then summarise how the magnitude, colour, and metallicity are combined with the classification to estimate a distance for each star.

Balmer line profiles. After normalising each spectrum to the continuum, we fit a Sérsic function, convolved with a Gaussian of FWHM the instrumental resolution, to the H δ and H γ lines. Two parameters of the fit, the scale width b , and the shape index c , are recorded. One classification procedure, the *Scale width–Shape* method, plots these two quantities against each other. A third quantity $D_{0.15}$, which is the line width at a depth 15% below the continuum, is derived from b and c . The second classification method, the *D_{0.15}–colour* method, plots this quantity against $(B - V)_0$. Because $D_{0.15}$ is a function of b and c , the two classification methods are not completely independent.

Metallicities from CaII K lines. The CaII K line is the strongest metal line present in the wavelength range covered by the spectra, and the only useful line in moderate resolution blue spectra for measuring metallicity. Plotting CaII K line EW against $(B - V)_0$, the metallicity is determined by interpolation between lines of constant metallicity on this diagram (see Fig. 4). The uncertainty is established from the uncertainties of the two quantities plotted, and an additional uncertainty of 0.3dex is added in quadrature. This is the systematic error, and was established by comparing metallicities derived by this method using high *S/N* data of comparable resolution, with accurate metallicities determined from high-resolution spectra. No attempt has been made to remove the possible contribution of interstellar CaII K absorption from the stellar K measurements. For a remote halo star the typical CaII K EW is 0.11 Å/sin b (Bowen, 1991), with a 95% range of (0.06 – 0.31) Å/sin b . This range translates to 0.07 – 0.35 Å for our fields. Our 34 stars have mean EW 1.7 Å and standard deviation 0.8 Å, with only two stars having EW below 0.7 Å. Therefore interstellar CaII K absorption is insignificant for the majority of

our targets, but could bias the measured metallicities high for the small fraction of stars with the weakest lines.

Distances. The absolute magnitude of a BHB star $M_V(BHB)$ depends on both metallicity and colour (i.e. temperature). In Paper II we derived a relation for the absolute magnitude of BHB stars by combining published relations for the dependence of M_V on metallicity and on $(B - V)_0$ colour, with the measured absolute magnitude at fixed metallicity and colour, as follows. The slope of the relation between apparent magnitude and metallicity for RR Lyrae stars in the Large Magellanic Cloud was measured by Clementini (2003) from observations of some 100 stars. We combined this with the measurement of the absolute magnitude of RR Lyrae stars at fixed metallicity, determined by Gould & Popowski (1998) from Hipparcos statistical parallaxes, to derive the linear relation for RR Lyrae stars:

$$M_V(RR) = 1.112 + 0.214[\text{Fe}/\text{H}]. \quad (4)$$

We then adopted a cubic expression determined by Preston et al. (1991), for the $(B - V)_0$ colour dependence of the difference in absolute magnitudes between BHB and RR Lyrae stars, to produce the final expression for the absolute magnitude of BHB stars:

$$\begin{aligned} M_V(BHB) = & 1.552 + 0.214[\text{Fe}/\text{H}] - 4.423(B - V)_0 \\ & + 17.74(B - V)_0^2 - 35.73(B - V)_0^3. \end{aligned} \quad (5)$$

Distances and associated errors are then determined using the apparent magnitudes V_0 , and the corresponding photometric and metallicity errors. To compute V , we used the relation $V = g' - 0.53(g' - r')$ (Fukugita et al., 1996), here disregarding the subtle differences between the different SDSS magnitudes (g, g', g^* , etc.). The result produces distance errors of 6 – 10% for our confirmed BHB stars. The exact form of Equation 5, particularly the zero point, remains controversial. Currently there are at least ten methods of determining the absolute magnitudes of RR Lyrae stars. We refer the interested reader to a recent review of this subject by Cacciari & Clementini (2003).⁴

The absolute magnitudes of blue stragglers have been less well studied. Since we will not use the blue stragglers in any dynamical analysis, their distances are less interesting. In Paper II we adopted the following relation derived by KSK from data for blue stragglers in globular clusters published by Sarajedini (1993)

$$M_V(BS) = 1.32 + 4.05(B - V)_0 - 0.45[\text{Fe}/\text{H}]. \quad (7)$$

3.3 Results

The results of these measurements for the 34 candidate BHB stars are provided in Table 3. Column (1) gives the number of the star, and columns (2) and (3) record the EW of the H γ line, and the spectrum continuum *S/N* per Å. Our classification methods were developed specifically for objects with strong Balmer lines, defined by $\text{EW H}\gamma > 13$ Å, and with continuum $\text{S/N} > 15$ Å⁻¹. In all, only 20 of the 34 candidates meet both criteria, and are therefore classifiable. The

⁴ They find, by averaging over all ten methods in their review,

$$M_V(RR) = 0.93 \pm 0.12 + (0.23 \pm 0.04)[\text{Fe}/\text{H}] \quad (6)$$

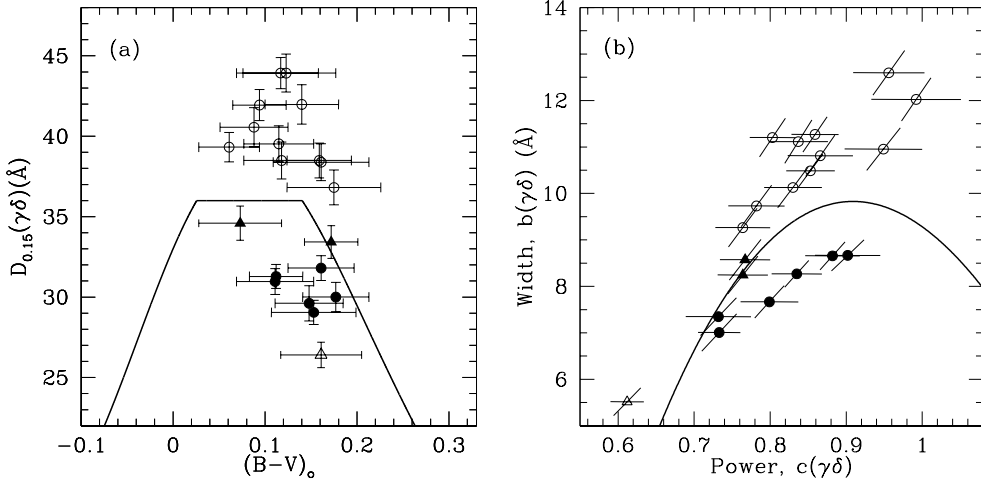


Figure 5. Classification of the 20 survey stars, using the $D_{0.15}$ -Colour (a) and the Scale width-Shape (b) classification methods. The solid curves are the classification boundaries explained in the text. Filled circles are stars classified BHB in both plots, i.e. the stars below the classification boundary in each plot. Filled triangles are stars below the classification boundary in only one plot but are nonetheless classified BHB, whereas open triangles are classified A/BS. In plot (a) there are eight stars below the boundary and 12 above it. In plot (b) there are seven stars below the boundary and 13 above it. A total of eight stars are classified BHB.

ID	RA (J2000)	Dec.	V	$(B - V)_0$	V_{\odot} [km s $^{-1}$]	$D_{0.15}(\gamma\delta)$ [Å]	$b(\gamma\delta)$ [Å]	$c(\gamma\delta)$	A	B	θ
M5-I-53	J151836.35 + 020744.6		15.06	0.06	52.2 ± 1.4	29.47 ± 0.26 29.38 ± 0.28	8.22 8.14	0.91 0.90	0.11 0.11	0.014 0.014	1.511 1.511
M5-II-78	J151826.93 + 020717.8		14.95	0.12	42.2 ± 1.1	27.81 ± 0.28 28.22 ± 0.28	7.58 7.65	0.87 0.87	0.11 0.12	0.015 0.014	1.509 1.511
M5-IV-05	J151835.34 + 020227.9		15.15	0.15	56.9 ± 1.2	29.51 ± 0.28 29.66 ± 0.27	8.07 8.12	0.88 0.89	0.11 0.11	0.014 0.013	1.512 1.512

Table 2. Spectroscopic measurements of three M5 globular cluster BHB stars. The names are from Arp (1955) and Arp (1962), the photometry is from Cudworth (1979), and the radial velocities are from Peterson (1983).

majority fail because of inadequate S/N . The information in successive columns (4) to (9) in Table 3 contain averages of $H\delta$ and $H\gamma$ line measurements. The quantities in columns (4) to (9) in Table 3, i.e. $D_{0.15}$, b , and c , A , B and θ , are also provided for the radial velocity standards in columns (6) to (11) of Table 2. Comparing these quantities enables us to use the observations of the standard stars as a further check of our classification methods.

In column (10) of Table 3 is listed the EW of the CaII K line. This is plotted against $(B - V)_0$ in Fig. 4. The measured metallicity for each star, and the error (including random and systematic contributions) is provided in column (11). The large errors are a consequence of the comparatively large errors in the $g^* - r^*$ colours. The mean measured metallicity of the stars plotted is -1.4 with dispersion 0.6, similar to the mean value measured for our sample of brighter A-type stars (Paper II). There are no significant outliers, but this is not a strong statement, given the large errors.

The radial velocity, corrected to the heliocentric frame, is provided in column (12), and the estimated distance,

based on the classification from the following section, is provided in column (13).

4 CLASSIFICATION AND VELOCITY DISPERSION

4.1 Classification

As noted above, of the 34 candidates, only 20 meet the requirements on spectroscopic S/N and $H\gamma$ EW for reliable classification. In the following we restrict our discussion to the classification of these 20 objects. Of the other 14 candidates, five stars have $\text{EW } H\gamma < 13\text{\AA}$, and are considered unclassifiable. For the remaining nine candidates the S/N of the spectra is too low for the classification to be reliable. We have nevertheless followed the classification procedures for these objects, but for clarity have omitted them from Figures 4 and 5. The final classifications are flagged as questionable. We have followed the classification procedures of Paper II (which are slightly different from those of Paper I) exactly, with the exception that we weight the two classification methods unequally, as detailed below.

No.	EW(γ) [Å]	S/N [Å] $^{-1}$	$D_{0.15}(\gamma\delta)$ [Å]	$b(\gamma\delta)$ [Å]	$c(\gamma\delta)$	A	B	θ	EW(CaIIK) [Å]	[Fe/H]	V_{\odot} [km s $^{-1}$]	R [kpc]	prob./class.
(1)	(2)	(3)	(4)	(5)	(6)	(7)	(8)	(9)	(10)	(11)	(12)	(13)	(14)
01	19.2	10.3	35.78 ± 1.69	9.24	0.77	0.68	0.068	1.521	0.92 ± 0.19	-2.09 ± 0.41	86.6 ± 19.0	73.4 ± 5.6	(0.39) A/BS?
02	19.8	15.2	41.98 ± 1.23	11.12	0.84	0.47	0.039	1.532	0.34 ± 0.17	-2.87 ± 0.37	393.8 ± 12.4	26.6 ± 7.9	(0.00) A/BS
03	17.7	15.9	38.50 ± 1.15	10.95	0.95	0.46	0.051	1.523	1.14 ± 0.17	-1.64 ± 0.41	260.9 ± 12.7	36.3 ± 5.1	(0.09) A/BS
04	20.0	19.2	41.94 ± 0.97	11.27	0.86	0.38	0.031	1.529	0.50 ± 0.16	-2.32 ± 0.38	172.0 ± 10.9	30.2 ± 5.6	(0.00) A/BS
05	16.1	20.4	30.97 ± 0.81	8.67	0.90	0.33	0.043	1.507	0.93 ± 0.15	-1.78 ± 0.45	172.8 ± 16.4	98.5 ± 7.9	(0.97) BHB
06	18.8	15.7	39.53 ± 1.12	10.81	0.87	0.44	0.043	1.528	1.44 ± 0.17	-1.37 ± 0.43	354.3 ± 13.8	39.2 ± 5.5	(0.04) A/BS
07	19.1	14.5	38.75 ± 1.13	9.44	0.71	0.45	0.033	1.527	1.35 ± 0.17	-1.83 ± 0.49	$-35.5 \pm 0.9.8$	30.3 ± 6.8	(0.03) A/BS?
08	18.8	17.9	38.38 ± 1.14	9.73	0.78	0.45	0.037	1.526	0.79 ± 0.17	-2.29 ± 0.51	56.9 ± 16.5	27.0 ± 7.1	(0.08) A/BS
09	14.2	21.2	26.40 ± 0.79	5.52	0.61	0.30	0.022	1.511	1.88 ± 0.15	-1.35 ± 0.48	$45.0 \pm 0.9.4$	49.8 ± 7.6	(0.33) A/BS
10	20.4	15.0	43.93 ± 1.18	12.60	0.96	0.48	0.047	1.527	0.72 ± 0.17	-2.11 ± 0.55	64.5 ± 15.4	47.8 ± 9.9	(0.00) A/BS
11	19.0	12.6	39.75 ± 1.49	9.68	0.74	0.59	0.040	1.528	1.59 ± 0.18	-1.20 ± 0.42	133.1 ± 47.4	43.0 ± 5.0	(0.05) A/BS?
12	11.6	17.5	24.59 ± 0.89	5.71	0.70	0.34	0.024	1.507	2.55 ± 0.15	-0.81 ± 0.54	96.7 ± 15.2	98.1 ± 6.6	unclassifiable
13	16.8	12.3	35.49 ± 1.38	9.14	0.77	0.55	0.050	1.520	2.18 ± 0.18	-1.08 ± 0.57	160.2 ± 17.6	49.0 ± 6.9	(0.28) A/BS?
14	13.7	21.4	29.05 ± 0.75	7.01	0.73	0.40	0.040	1.514	2.19 ± 0.11	-1.14 ± 0.48	-21.2 ± 10.5	102.3 ± 5.1	(0.75) BHB
15	16.8	9.0	32.74 ± 1.87	7.95	0.74	0.77	0.059	1.518	2.86 ± 0.20	-0.50 ± 0.71	19.4 ± 24.5	91.4 ± 6.5	(0.52) BHB?
16	17.4	15.8	36.82 ± 1.08	9.26	0.76	0.42	0.036	1.526	0.80 ± 0.16	-2.36 ± 0.49	2.7 ± 10.7	40.3 ± 10.9	(0.15) A/BS
17	9.9	14.7	21.03 ± 1.17	4.18	0.57	0.40	0.042	1.492	2.98 ± 0.11	-0.80 ± 0.61	97.4 ± 16.9	101.5 ± 7.3	unclassifiable
18	19.2	19.9	39.32 ± 0.91	10.49	0.85	0.36	0.032	1.526	1.94 ± 0.16	-0.49 ± 0.46	58.3 ± 10.0	49.4 ± 3.3	(0.01) A/BS
19	15.0	16.8	33.42 ± 1.02	8.24	0.76	0.41	0.033	1.522	2.06 ± 0.16	-1.31 ± 0.41	38.3 ± 12.2	68.7 ± 4.8	(0.65) BHB
20	18.4	13.1	35.98 ± 1.41	8.63	0.72	0.56	0.041	1.525	1.28 ± 0.18	-1.68 ± 0.47	120.2 ± 13.4	46.2 ± 8.5	(0.24) A/BS?
21	19.2	15.7	40.56 ± 1.21	12.02	0.99	0.47	0.059	1.529	0.95 ± 0.17	-1.63 ± 0.38	-95.6 ± 20.0	42.1 ± 5.9	(0.01) A/BS
22	20.2	13.2	38.64 ± 1.57	8.84	0.67	0.60	0.037	1.530	3.13 ± 0.19	-0.38 ± 0.55	74.2 ± 22.5	58.5 ± 5.1	(0.06) A/BS?
23	16.1	13.9	34.92 ± 1.33	7.96	0.68	0.54	0.035	1.525	1.73 ± 0.18	-1.44 ± 0.45	-31.5 ± 16.6	44.2 ± 7.2	(0.29) A/BS?
24	13.7	21.9	31.28 ± 0.75	8.27	0.84	0.29	0.033	1.516	1.01 ± 0.15	-1.71 ± 0.36	18.0 ± 0.97	66.8 ± 5.0	(0.96) BHB
25	12.2	16.1	24.90 ± 1.08	5.55	0.66	0.41	0.037	1.508	2.79 ± 0.16	-0.87 ± 0.59	32.6 ± 16.8	104.3 ± 7.3	unclassifiable
26	13.2	12.3	31.07 ± 1.40	7.27	0.71	0.52	0.043	1.521	2.07 ± 0.18	-1.12 ± 0.53	78.3 ± 16.9	105.1 ± 8.0	(0.48) A/BS?
27	13.8	18.9	30.00 ± 0.91	7.67	0.80	0.35	0.038	1.515	1.36 ± 0.15	-1.81 ± 0.43	90.3 ± 08.9	78.5 ± 6.5	(0.94) BHB
28	15.2	16.0	29.61 ± 1.09	7.35	0.73	0.41	0.043	1.512	2.68 ± 0.16	-0.74 ± 0.49	88.8 ± 11.5	64.9 ± 4.0	(0.68) BHB
29	15.9	16.5	34.59 ± 1.06	8.57	0.77	0.44	0.033	1.523	1.83 ± 0.16	-0.69 ± 0.54	92.3 ± 12.7	76.8 ± 4.8	(0.51) BHB
30	10.5	11.2	25.17 ± 1.34	6.22	0.76	0.53	0.059	1.509	3.66 ± 0.18	-0.04 ± 0.54	47.4 ± 21.3	77.0 ± 4.3	unclassifiable
31	20.1	19.0	43.93 ± 0.97	11.20	0.80	0.42	0.030	1.530	1.28 ± 0.16	-1.51 ± 0.44	41.2 ± 11.3	47.0 ± 6.7	(0.00) A/BS
32	18.2	16.3	38.49 ± 1.09	10.13	0.83	0.44	0.038	1.525	2.50 ± 0.16	-0.96 ± 0.45	133.7 ± 12.9	40.1 ± 5.0	(0.08) A/BS
33	15.0	20.0	31.80 ± 0.77	8.66	0.88	0.30	0.036	1.516	0.96 ± 0.15	-2.05 ± 0.46	119.2 ± 12.3	80.0 ± 6.6	(0.98) BHB
34	11.6	13.5	27.81 ± 1.16	6.04	0.63	0.44	0.037	1.513	1.28 ± 0.17	-1.66 ± 0.44	104.5 ± 12.6	84.5 ± 6.6	unclassifiable

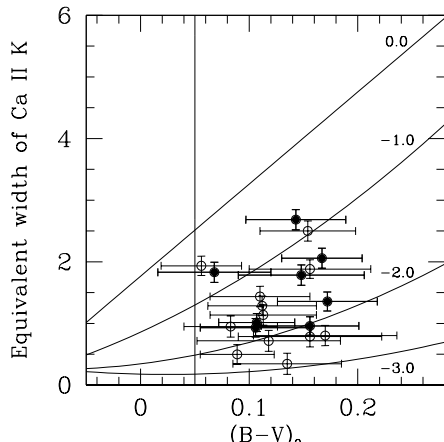
Table 3. Spectroscopic data for the horizontal branch star candidates.

Figure 4. CaII K line (3933 Å) EW(Å) for the sample plotted against $(B - V)_0$. The curves represent lines of constant metallicity for $[\text{Fe/H}] = -1.0, -2.0$ and -3.0 taken from Wilhelm et al. (1999). The straight line represents a best fit to stars in the Pleiades and Coma clusters assumed to be of solar metallicity. The vertical line at $(B - V)_0 = 0.05$ is the limit for which metallicities can be determined. The 8 stars classified as BHB stars are marked by filled circles, and the 12 stars classified blue stragglers are marked by open circles.

In Figure 5 we plot the two diagnostic diagrams for the 20 classifiable stars in the survey. The two figures are explained as follows. Figure 5(a) shows the $D_{0.15}$ –colour method. The average values of $D_{0.15}$ for $\text{H}\gamma$ and $\text{H}\delta$ against $(B - V)_0$ are plotted for the 20 candidates. In Paper I we showed that reliable classification by this method requires the uncertainty on $(B - V)_0$ to be less than 0.03 mag. Unfortunately this is untrue for most of the stars in our sample (Table 1). For this reason we give this method lower weight

in the final classification. Figure 5(b) shows the *Scale width–Shape* method. The line-profile quantities b and c , averaged for $\text{H}\gamma$ and $\text{H}\delta$ are plotted. The solid lines show the classification boundaries, from Paper II, with high-surface gravity stars (i.e. main-sequence A stars or blue stragglers, hereafter A/BS) above the line, and low-surface gravity stars (i.e. BHB stars) below the line. In both plots stars classified BHB are plotted as solid symbols and stars classified A/BS are plotted open. As we discuss below, the three triangles are stars that have ambiguous classifications, i.e stars that are classified as BHB by one classification method and not the other.

Inspection of Figure 5 provides the following information. Of the 20 candidates, eight are classified BHB by the $D_{0.15}$ –colour method. The *Scale width–Shape* method classifies seven stars as BHB. There are six stars classified BHB by both methods. A total of nine stars are classified BHB by one or other of the methods. There is clearly close agreement between the two classification methods, but there are three stars with ambiguous classifications. Before considering these further, we note that the three radial velocity standards (Table 2), previously classified BHB from high-resolution spectroscopy, are all unambiguously classified BHB in both plots.

The uncertainties on each parameter define the 2D probability distribution functions for any point. By integrating these functions below the classification boundary we can compute a probability $P(\text{BHB})$ that any star is BHB. We can then average the probabilities for the two classification methods, to improve the classification. We have computed these probabilities for each star, giving twice the weight to the *Scale width–Shape* method when averaging (because, as mentioned above, the $D_{0.15}$ –colour method is affected by the relatively large colour errors). As in previous papers, stars with $\bar{P}(\text{BHB}) > 0.5$ are then classified BHB, and

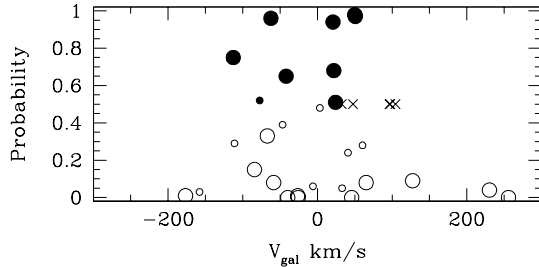


Figure 6. Classification probability against V_{gal} for all the BHB candidates. Large circles represent the 20 stars with spectra of high S/N . The BHB stars which have $\bar{P} > 0.5$ are shown by filled symbols and A/BS stars are marked by open symbols. Also plotted, as small symbols, are the nine stars with unreliable classifications. Finally the five unclassifiable stars are marked by small crosses, at $\bar{P} = 0.5$.

stars with $\bar{P}(BHB) \leq 0.5$ are classified A/BS. Based on the Monte Carlo simulations of Paper I, we would expect the sample of BHB stars defined in this way to be contaminated by A/BS stars at no more than the 10% level, which we consider satisfactory. Col. (14) of Table 3 provides the averaged probabilities, and corresponding classifications, for the 20 classifiable stars.

Of the three stars with ambiguous classifications, 2 are classified BHB. The third star classified A/BS, star 9, is the object with the smallest value of $D_{0.15}$, and the smallest value of c . The small value of c indicates a colour substantially redder than (although compatible with) the measured value of $(B - V)_0 = 0.16 \pm 0.04$.

We also provide the classification probabilities for the nine stars with inadequate spectroscopic S/N , but for these the classifications are given as BHB? or A/BS? to indicate that they are not reliable. Finally the five stars with $EW_{H\gamma} < 13\text{\AA}$ are labelled unclassifiable.

4.2 Velocity dispersion

Table 4 contains a summary of the kinematic properties of the final sample of eight BHB stars. Listed there are the Galactic coordinates l and b , and the Galactocentric radial velocity and distance, V_{gal} and r respectively. To convert the heliocentric quantities to Galactocentric quantities, the heliocentric radial velocities are first corrected for solar motion by assuming a solar peculiar velocity of $(U, V, W) = (-9, 12, 7)$, where U is directed outward from the Galactic Centre, V is positive in the direction of Galactic rotation at the position of the Sun, and W is positive toward the North Galactic Pole. We have assumed a circular speed of 220 km s^{-1} at the Galactocentric radius of the Sun ($R_\odot = 8.0$ kpc). Table 4, then, distills the main observational result of the paper, a sample of distant BHB stars with measured radial velocities. The Table also includes three carbon stars, designated by their coordinates, which are introduced in Section 5.

We find, after quadratically subtracting the measurement errors in the same manner as Norris & Hawkins (1991), that the measured dispersion of the radial component of the Galactocentric velocity dispersion for our BHB sample is

No.	l [$^\circ$]	b [$^\circ$]	V_{gal} [km s^{-1}]	r [kpc]
19	301.495	63.377	-42.0	67.2
24	304.106	62.463	-62.3	65.1
27	310.805	63.473	20.8	76.6
28	312.874	63.489	21.9	62.9
29	313.702	62.623	24.2	74.7
34	315.536	61.130	49.9	77.6
1225-0011	290.267	61.822	-27.0	65.0
1241+0237	298.280	65.159	-32.0	66.0
1249+0146	303.159	64.372	-133.0	53.0
05	262.690	56.439	50.7	99.4
14	289.614	63.028	-112.7	101.4

Table 4. Summary of kinematic information for the BHB and carbon stars that are associated with the stream. The two BHB stars below the line do not belong to the stream.

58 ± 15 km s^{-1} at a mean heliocentric distance of 80 kpc. In Table 5 we compare this value against the measured velocity dispersion of a variety of samples. The sample of remote BHB stars is referred to as Sample A, and listed in the first line of Table 5. The first comparison sample, Sample B, comprises the 60 BHB stars $11 < R < 52$ kpc, mean $R = 28$ kpc, from Paper II, which is the largest sample at such distances. Sirko et al. (2004a) have also isolated large samples of distant BHB stars using the SDSS. They split their sample into a bright ($g < 18$) subsample, which is contaminated by blue stragglers at the level of about 10% (i.e. similar to the work presented here), and a faint subsample ($g > 18$), which is contaminated at about 25%. If we consider only their clean bright sample, here Sample C, then $\sigma = 99.4 \pm 4.3$ km s^{-1} (Sirko et al. 2004b), at mean distance 16 kpc. Sample D consists of the 12 stars in Table 3 classified BS, with measured velocity dispersion 129 ± 26 km s^{-1} , at mean distance 40 kpc. Finally considering the Galactic satellites discussed in §1, selecting the nine satellites within the distance range of our remote BHB sample, i.e. $65 < R < 102$ kpc, Sample E, we measure a velocity dispersion 134 ± 32 km s^{-1} , at a mean distance 82 kpc. The velocity dispersions, mean distances, and sample sizes, of these four samples are entered in columns 2 – 4 of Table 5. In the final column we list the probability that the measured value for the remote BHB stars could be drawn from the same population as each of the four comparison samples, as measured by the F-test. At better than the 95% significance level, our sample of remote BHB stars has smaller velocity dispersion than BHB stars at much smaller radii (16 kpc, Sample C), BS stars of similar apparent magnitude at intermediate radii (40 kpc, Sample D), and satellites at the same radii (82 kpc, Sample E). Compared to the sample of BHB stars at 28 kpc, the difference is not significant. We conclude that the velocity dispersion of the remote BHB stars is anomalously low, and in the following section we seek an explanation.

5 DISCUSSION

In considering the anomalously low velocity dispersion of the remote BHB stars, we first check that the significantly

Sample	Population	Dispersion [km s ⁻¹]	$\langle R \rangle$ [kpc]	Size	F-test [prob.]
A	BHB	58 ± 15	80	8	...
B	BHB	108 ± 10	28	60	0.09
C	BHB	99.4 ± 4.3	16	733	0.02
D	BS	129 ± 26	40	12	0.02
E	satellites	134 ± 32	82	9	0.04

Table 5. Comparison of measured velocity dispersion of a variety of populations in the Galactic halo, against the measured velocity dispersion of our new sample of eight remote BHB stars at mean distance ($\langle R \rangle$) of 80 kpc, Sample A.

different velocity dispersion between the BHB and BS stars is robust. In Fig. 6 we plot classification probability against V_{gal} . In this plot, the large symbols represent the 20 stars with spectra of high S/N . BHB stars have $\bar{P} > 0.5$, and, as usual, are shown by filled symbols, with A/BS stars marked by open symbols. Also plotted, as small symbols, are the nine stars with unreliable classifications. Finally the five unclassifiable stars are marked by small crosses, at $\bar{P} = 0.5$. This plot shows a clear difference in the kinematics of stars at the bottom of the diagram (high probability A/BS, large velocity spread), and at the top of the diagram (high probability BHB, small velocity spread). There is no evidence for any BHB stars with large values of $|V_{gal}|$ that have been missed, because they fall just outside the classification boundary, or because they were unclassifiable because the spectra are of low S/N . Therefore, the difference in velocity dispersion between the two populations is quite robust to the method of classification.

Another concern we had was the possibility that the sample is contaminated by misclassified blue stragglers in the Sagittarius stream. Fig. 2 plots α against g^* of the initial list of candidate BHB stars. As we discussed earlier this colour-selected sample of candidates is expected to be contaminated by blue stragglers, because of the large photometric errors at these faint magnitudes, and this is apparently confirmed by the high-density of stars at $\alpha > 200^\circ$, where presumably most of the stars are blue stragglers. It was therefore worrying that the eight BHB stars, marked in the upper diagram by filled circles, mostly lie close to the boundary $\alpha = 200^\circ$ in this plot, whereas one might expect them to be more uniformly scattered over the RA range. If these stars are misclassified blue stragglers, on the edge of the Sagittarius stream, this would provide a natural explanation for the small velocity dispersion. However, if there are any Sagittarius blue stragglers $\alpha < 200^\circ$ in our candidate list, most will be classified blue straggler, and the reduction in velocity dispersion would be greatest in our A/BS sample – the opposite of what is seen.

We conclude from the foregoing discussion that we have succeeded in defining samples of BHB and A/BS stars, with small contamination, that show distinct kinematic properties. Indeed the fact that the measured velocity dispersions of the two populations are significantly different is confirmation of the reliability of the classification methods. In seeking an explanation for this difference, a number of possible dynamical explanations could be pursued, for example that the stellar orbits change from being predominantly radial to predominantly circular at large radii (e.g. Sommer-Larsen et al.

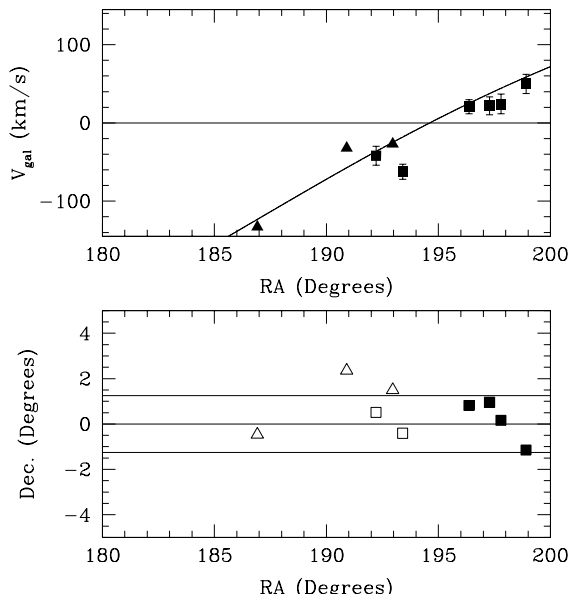


Figure 7. *Upper:* Plot of V_{gal} versus RA for the six BHB stars (shown as solid squares) and three carbon stars (solid triangles) that are potential members of a stream. The plot suggests that these stars are located near the turning point of an orbit (where the radial velocity changes sign). The turning point is located at an RA of about 195° . *Lower:* A plot of RA versus Dec. for the stars in the stream. The filled symbols are the stars with $V_{gal} > 0$ and the open symbols are for $V_{gal} < 0$ otherwise the symbols are the same as in the upper plot. The BHB stars are confined to the northern stripe of the EDR data set shown by the horizontal lines.

1997). While this is possible, a more convincing explanation was immediately apparent.

Six of the BHB stars are confined to a small region of space with $190^\circ < \alpha < 200^\circ$, $63 < r < 78$ kpc (and a small range in δ). The average distance of these stars from the centre of the Galaxy is 70.6 kpc. These stars are therefore confined to a very small fraction of the volume surveyed. The velocity dispersion of these six stars (corrected for measurement errors), 42 ± 12 km s⁻¹, is too large to associate them with a bound object i.e. a low surface-brightness dwarf galaxy. The key to understanding the anomalous velocity dispersion is provided in Figure 7(upper), which plots Galactocentric radial velocity V_{gal} versus RA for these six BHB stars, marked by squares. A correlation is evident, indicative of streaming motion, perhaps associated with a dis-

rupted satellite. Figure 7(lower) plots the position on the sky of the six stars. To investigate further the possibility of a stream, we searched the catalogue of faint carbon stars of Totten & Irwin (1998) in the vicinity, confining ourselves to the ranges $\text{RA } 160^\circ < \alpha < 200^\circ$, $\text{Dec. } \pm 5^\circ$, and to similar distances (improved distance estimates taken from Totten, Irwin & Whitelock, 2000). Three stars meet these criteria, and have been added to both diagrams in Figure 7, marked as triangles. Remarkably the three stars appear to add to the evidence of a stream. Details of the three stars are provided in Table 4. (The velocity errors, taken from Totten, Irwin & Whitelock (2000), are 4, 4 and 6 km s^{-1} in the order the stars appear in the Table)

The correlation between V_{gal} and RA evident in Figure 7(upper), encompasses $V_{\text{gal}} = 0$, which would correspond to a turning point in the orbit at RA of $\sim 195^\circ$. In order to investigate this trend in more detail, we consider orbits in the spherical potential

$$\Psi(r) = \frac{GM}{a} \log \left[\frac{\sqrt{a^2 + r^2} + a}{r} \right]. \quad (8)$$

The scale length $a = 178.0 \text{ kpc}$ and the mass $M = 2.0 \times 10^{12} M_\odot$ are chosen to match those estimated for the halo of the Milky Way (Wilkinson et al. 2003). We investigate whether the trend in Figure 7 can be reproduced by a plausible Galactic orbit as follows. First, we assume that the orbit has a turning point in the RA range $190 - 200^\circ$ and in the distance range $50 - 80 \text{ kpc}$. We then choose values for the line-of-sight distance d_0 , Galactic latitude b_0 and longitude l_0 of the turning point and the values of the two components of velocity transverse to the line of sight, $v_{\text{b},0}$ and $v_{\text{l},0}$. From each set of initial conditions, we integrate the orbit in the RA range $190 - 200^\circ$ and determine $V_{\text{gal}}(\text{RA})$. Assuming Gaussian errors σ_i on the individual radial velocities (and neglecting any errors in the RA measurements), the probability that the data $(V_{\text{gal},i}, \text{RA}_i)$ were drawn from the relation $V_{\text{gal}}(\text{RA})$ is given by

$$P(v_{\text{los},i}, \text{RA}_i | l_0, b_0, r_0, v_{\text{b},0}, v_{\text{l},0}) = \prod_i \frac{1}{\sqrt{2\pi\sigma_i^2}} \exp \left[-\frac{(v_{\text{los}}(\text{RA}_i) - v_{\text{los},i})^2}{2\sigma_i^2} \right]. \quad (9)$$

We use a downhill simplex algorithm (the routine `amoeba` in Press et al. 1992) to maximise this probability over the five dimensional parameter space. The resulting $V_{\text{los}}(\text{RA})$ relation is shown in Figure 7. The orbit we obtain is strongly radial and has an apocentre of 67.1 kpc and pericentre of 7.5 kpc . The energy and angular momentum of the orbit are $E = -8.1 \times 10^4 (\text{km s}^{-1})^2$ and $L^2 = 1.2 \times 10^7 (\text{kpc km s}^{-1})^2$. The velocity dispersion of all nine stars relative to this orbit is $15 \pm 4 \text{ km s}^{-1}$.

Up to this point, we have not made use of the estimated distances to our tracer stars, due to their relatively large uncertainties. We can include them in the orbit determination in a straightforward manner by multiplying the probability in eq (9) by a second Gaussian $P(d_{\text{los}})$ given by

$$P(d_{\text{los},i}, \text{RA}_i | l_0, b_0, r_0, v_{\text{b},0}, v_{\text{l},0}) = \frac{1}{\sqrt{2\pi\sigma_{d,i}^2}} \exp \left[-\frac{(d_{\text{los}}(\text{RA}_i) - d_{\text{los},i})^2}{2\sigma_{d,i}^2} \right]. \quad (10)$$

Here, $\sigma_{d,i}$ is the uncertainty in the line of sight distance

to the i th star. In fact, the inclusion of this term results in an almost identical orbit, the distance uncertainties rendering the distance estimates of little value in the determination of orbital parameters.

We initially analysed the data using the technique of Lynden-Bell & Lynden-Bell (1995). These authors note that if a group of stars lie on the same orbit in an assumed spherical potential, they share the same energy E and total angular momentum L^2 . Since the energy is given by

$$|E| = \Psi(r) - \frac{1}{2}v_r^2 - \frac{1}{2}\frac{L^2}{r^2}, \quad (11)$$

where v_r is the Galactocentric radial velocity, L is the magnitude of the total angular momentum vector and $\Psi(r)$ is the potential, the stars in a stream lie on a straight line in a plot of $|E_r|$ versus r^{-2} where

$$|E_r| = \Psi(r) - \frac{1}{2}v_r^2. \quad (12)$$

If we apply this technique to our data, we obtain orbits with very significantly higher orbital angular momenta than that for the orbit which fits the V_{gal} versus RA relation above. After consideration of the propagation of the observational errors into the $(|E_r|, 1/r^2)$ plane, we noted that the orbital angular momentum was in fact being governed by the orientation of the extended error ellipses caused by the large distance uncertainties. In addition, the derived orbit does not reproduce the trend of V_{gal} with RA seen in Figure 7. We conclude therefore that this technique can only yield useful information about an orbit if the magnitudes of the distance errors are significantly smaller than the radial range covered by the survey – this is not the case for our present sample.

Given the proximity of the Sagittarius (Sgr) stream, it is reasonable to suppose the BHB stars might be part of a more distant passage of the stream around the Milky Way (e.g. Helmi & White 2001; Dohm-Palmer et al. 2001). Comparing the positions and heliocentric velocities of our sample of stars to the simulations plotted in Dohm-Palmer et al. (2001; their figure 3) reveal that our sample largely lies either between or beyond two wraps of the Sgr stream. In fact, two of our six BHB stream stars (numbers: 34 and 28) are inconsistent with the model simulations. More recently, Law, Johnston & Majewski (2005) produced models of the Sgr tidal tails using test particle orbits and N -body simulations in a variety of potentials. Before we are able to compare our data with these models we need to convert our coordinates to the system defined in Majewski et al. (2003). In this coordinate system the zero plane of the latitude coordinate B_\odot coincides with the best-fit great circle defined by the Sgr debris, as seen from the Sun; the longitudinal coordinate Λ_\odot is zero in the direction of the Sgr core and increases along the Sgr trailing stream. Our sample resides in the region $249^\circ < \Lambda_\odot < 275^\circ$ and $7^\circ < B_\odot < 20^\circ$. At these coordinates the whole sample of stars in Table 4 resides at larger distances than the models predict. Clearly, the observation of a larger sample of remote BHB stars in the Galaxy halo, along different lines of sight, is essential to confirm the reality of the stream. Additionally, we need to establish whether the small velocity dispersion measured for the eight distant BHB stars discovered in this paper is actually because six of the stars are associated with a coherent structure, or because the velocity dispersion of the

whole population of outer halo BHB stars falls steeply with radius. However, we note that the apparent dominance of streaming motion in our BHB sample lends support to the claim of Majewski (2004) that the non-uniform kinematics of outer halo K-giants are consistent with that population having derived almost completely from accretion.

We close with a summary of the main points of this paper. We have presented the results of a survey of remote halo A-type stars selected from the SDSS. Spectroscopy of the A-type stars obtained with the VLT produced a sample of 20 stars with data of suitable quality for classification into the classes BHB and A/BS. The final sample (Table 4) comprises eight stars classified BHB, at distances of $65 - 102$ kpc from the Sun (mean distance 80 kpc), with heliocentric radial velocities accurate to 12 km s^{-1} , on average, and distance errors $< 10\%$. This is the most distant sample of Galactic stars with measured radial velocities, of this size. Of the eight remote BHB stars, we find that six show a strong trend in V_{gal} with RA, and are consistent with a single orbit in a spherical halo potential. The measured dispersion of the radial component of the Galactocentric velocity for this sample is $42 \pm 12 \text{ km s}^{-1}$. This value is significantly smaller than values measured for samples of stars at smaller radii, and for satellites at similar radii. This evidence is supported by the existence of three previously identified carbon stars with the same kinematics. A simple model shows all the stars lying on an orbit with energy and angular momentum of $E = -8.1 \times 10^4 (\text{km s}^{-1})^2$ and $L^2 = 1.2 \times 10^7 (\text{kpc km s}^{-1})^2$. The velocity dispersion of the nine stars is $56 \pm 13 \text{ km s}^{-1}$; the dispersion relative to the calculated orbit is $15 \pm 4 \text{ km s}^{-1}$. We conclude that we find a strong indication of the presence of a stream but further observations are required to trace the full extent of this stream on the sky.

ACKNOWLEDGEMENTS

We thank Kyle Cudworth for providing us with accurate positional information for the radial velocity stars in M5, and J.A.Smith for supplying us with photometric data. We also thank Mike Irwin for several valuable discussions and for pointing us towards the carbon star data set of Totten & Irwin. The Sgr coordinate system conversions made use of code at: <http://www.astro.virginia.edu/~srm4n/Sgr/code.html>. We are grateful to the referee for comments that helped improved the clarity of the manuscript. LC and MIW acknowledge PPARC for financial support. This paper uses observations made on the Very Large Telescope at the European Southern Observatory, Cerro Paranal, Chile [programme ID: 71.B-0124(A)]. We made use of the SDSS online database. Funding for the creation and distribution of the SDSS Archive has been provided by the Alfred P. Sloan Foundation, the Participating Institutions, the National Aeronautics and Space Administration, the National Science Foundation, the U.S. Department of Energy, the Japanese Monbukagakusho, and the Max Planck Society.

REFERENCES

Abazajian K. et al., 2004, AJ, 128, 502
 Arp H. C., 1955, AJ, 60, 317
 Arp H. C., 1962, AJ, 135, 311
 Bowen, D. W., 1991, MNRAS, 251, 649
 Cacciari C., Clementini G., LNP, 635, 105
 Clementini G., Gratton R., Bragaglia A., Carretta E., Di Fabrizio L., Maio M., 2003, ApJ, 125, 1309
 Clewley L., Warren S.J., Hewett P.C., Norris J.E., Peterson R.C., Evans N.W., 2002, MNRAS, 337, 87 (Paper I)
 Clewley L., Warren S.J., Hewett P.C., Norris J.E., Evans N.W., 2004, MNRAS, 352, 285 (Paper II)
 Cudworth K.M., 1979, AJ, 84, 1866
 Dohm-Palmer R.C. et al., 2001, ApJ, 555, L37
 Fukugita M. et al., 1996, AJ, 111, 1748
 Gould A., Popowski P., 1998, ApJ, 508, 844
 Helmi A., White S. D. M., 2001, MNRAS, 323, 529
 Ibata R. A., Gilmore G. and Irwin M. J., 1994, Nature, 370, 6486, 194
 Ibata R., Chapman S., Ferguson A.M.N., Irwin M., Lewis G., McConnachie A., 2004, MNRAS, 351, 117
 Irwin M., Hatzidimitriou D., 1995, MNRAS, 277, 1354
 Johnston K.V., Zhao H., Spergel D.N., Hernquist L., 1999, ApJ, 512, L109
 Kinman T.D., Suntzeff N.B., Kraft R.P., 1994, AJ, 108, 1722
 Kurucz R., 1993, CD-ROM No.13, Smithsonian Astrophysical Observatory
 Law D.R., Johnston K.V., Majewski S.R., 2005, ApJ, 619, 807
 Lewis G.F., Ibata R.A., Chapman S.C., Ferguson A.M.N., McConnachie A.W., Irwin M.J., Tanvir N., 2004, PASA, 21, 203
 Lenz D. D., Newberg J., Rosner R., Richards G. T., Stoughton C., 1998, ApJS, 119, 121
 Lynden-Bell D., Lynden-Bell R. M., 1995, MNRAS, 275, 429
 Majewski et al. 2003, ApJ, 599, 1082
 Majewski S.R., 2004, Publications of the Astronomical Society of Australia, 21, 197
 Norris J.E., Hawkins M.R.S., 1991, ApJ, 380, 104
 Peterson R.C, 1983, ApJ, 275, 737
 Press W. H., Teukolsky S.A., Vetterling W.T., Flannery B.P., Numerical recipes in C. The art of scientific computing, Cambridge University Press, Cambridge, 1992, 2nd edition
 Preston G.W., Shectman S.A., Beers T.C., 1991, ApJ, 375, 121
 Sanduleak N., 1980, PASP, 92, 246
 Sarajedini A., 1993, in Saffer R. A., ed., ASP Conf. Ser. Vol. 53, Blue Stragglers. Astron. Soc. Pac., San Francisco, p. 14
 Schlegel D.J., Finkbeiner, D.P., Davis, M., 1998, ApJ, 500, 525
 Sirko E., Goodman J., Knapp G.R., Brinkmann J., Ivezić, Ž., Knerr E.J., Schlegel D., Schneider D.P., York D.G., 2004a, AJ, 127, 899
 Sirko E., Goodman J., Knapp G.R., Brinkmann J., Ivezić, Ž., Knerr E.J., Schlegel D., Schneider D.P., York D.G., 2004b, AJ, 127, 914
 Smith, J. A. et al. 2002, AJ, 123, 2121

Sommer-Larsen J., Beers T. C., Flynn C., Wilhelm R., Christensen P. R., 1997, ApJ, 481, 775
Stoughton, C. et al. 2002, AJ, 123, 485
Totten, E.J., Irwin, M.J., 1998, MNRAS, 294, 1
Totten, E.J., Irwin, M.J., Whitelock, P.A., 2000, MNRAS, 314, 630
Wilkinson M.I., Kleyna J.T., Evans N.W., Gilmore, G., 2003, in Bender R. Renzini A. eds., “The Mass of Galaxies at Low and High Redshift”, ESO Astrophysics Symposia, 10
Wilhelm R., Beers T.C., Gray R.O., 1999, AJ, 117, 2308
Yanny B. et al., 2000, AJ, 540, 825 (Y2000)